hydrology

MDPI

Article

Quantification of Mountainous Hydrological Processes in the Aktash River Watershed of Uzbekistan, Central Asia, over the Past Two Decades

Ying Ouyang [1,*], John A. Stanturf [2,3], Marcus D. Williams [4], Evgeniy Botmann [5] and Palle Madsen [3]

1 USDA Forest Service, Center for Bottomland Hardwoods Research, Southern Research Station, 775 Stone Blvd., Thompson Hall, Room 309, Mississippi State, MS 39762, USA
2 Institute of Forestry and Engineering, Estonian University of Life Sciences, 51014 Tartu, Estonia; johnalvin.stanturf@emu.ee
3 InNovaSilva, ApS, 7100 Vejle, Denmark; palle@innovasilva.com
4 Center for Forest Health and Disturbance, US Forest Service, Athens, GA 30602, USA; marcus.d.williams@usda.gov
5 Research Institute of Forestry, Tashkent 100174, Uzbekistan; darhanbek@yandex.ru
* Correspondence: ying.ouyang@usda.gov

Abstract: Estimation of hydrological processes is critical to water resource management, water supply planning, ecological protection, and climate change impact assessment. Mountains in Central Asia are the major source of water for rivers and agricultural practices. The disturbance of mountain forests in the region has altered the hydrological processes and accelerated soil erosion, mudflow, landslides, and flooding. We used the SWAT (Soil and Water Assessment Tool) model calibrated and validated with remote sensing data to quantify the mountainous hydrological processes in the Aktash River watershed (ARW) of Uzbekistan, Central Asia. Simulations showed that the daily surface runoff and streamflow closely responded to daily precipitation. Groundwater discharge reached its maximum in winter because of snowmelt. The wet months were from July to December, and the dry months were from January to June. The magnitudes of the seasonal hydrological processes were in the following order: fall > summer > winter > spring for precipitation and surface runoff; summer > spring > fall > winter for evapotranspiration (ET); winter > spring > fall > summer for snowmelt; fall > winter > summer > spring for water yield and streamflow; and winter > fall > spring > summer for groundwater discharge. The Mann–Kendall statistical test revealed a significant increasing trend for the annual precipitation ($\tau = 0.45$, $p < 0.01$) and surface runoff ($\tau = 0.41$, $p < 0.02$) over the past 17 years from 2003 to 2019. Compared to rangeland, forested land decreased monthly and annual average surface runoff by 20%, and increased monthly and annual average groundwater recharge by about 5%. Agricultural land had much higher unit-area values (mm/km^2/y) of ET, groundwater recharge, and water yield than those of urban, forest, and range lands. Our research findings provide useful information to farmers, foresters, and decision makers for better water resource management in the ARW, Central Asia, and other mountain watersheds with similar conditions.

Keywords: Central Asia; hydrological processes; mountain watershed; SWAT model

check for updates

Citation: Ouyang, Y.; Stanturf, J.A.; Williams, M.D.; Botmann, E.; Madsen, P. Quantification of Mountainous Hydrological Processes in the Aktash River Watershed of Uzbekistan, Central Asia, over the Past Two Decades. *Hydrology* **2023**, *10*, 161. https://doi.org/10.3390/hydrology10080161

Academic Editors: Nikolaos Proutsos and Stefanos Stefanidis

Received: 5 July 2023
Revised: 20 July 2023
Accepted: 27 July 2023
Published: 2 August 2023

Copyright: © 2023 by the authors. Licensee MDPI, Basel, Switzerland. This article is an open access article distributed under the terms and conditions of the Creative Commons Attribution (CC BY) license (https://creativecommons.org/licenses/by/4.0/).

1. Introduction

Estimation of hydrological processes is central to water resource management, water supply planning, ecological protection, and climate change impact assessment. In water resource management, hydrological processes, such as surface runoff and streamflow, are used to issue discharge permits. In water supply planning, hydrological processes are used to determine allowable water transfers and withdrawals. In ecological protection, hydrological processes are employed to assess terrestrial and aquatic habitats. In climate change impact assessment, patterns and variations of hydrological processes are critical indicators of climate variability [1].

Situated at the center of the Eurasian continent, Central Asia is typically understood to mean the whole of five former Soviet republics: Kazakhstan, Kyrgyzstan, Tajikistan, Turkmenistan, and Uzbekistan. The region consists of about four million km^2 [2,3] and has a strong arid to semiarid continental climate that varies with elevation within the countries [4]. The average annual precipitation is 250 mm in Uzbekistan and 500 mm in Tajikistan [5]. Annual potential evapotranspiration varies from more than 2250 mm in the most arid area to less than 500 mm in the mountains [6,7]. The mean temperature ranges from −3 to 20 °C in winter and 20 to 40 °C in summer, while the minimum winter temperature can drop to −45 °C and the maximum summer temperature can be up to 50 °C [8].

Kyrgyzstan and Tajikistan are mountainous countries, with more than 90% of their national territories mountainous, while Uzbekistan, Kazakhstan, and Turkmenistan have smaller mountainous regions. The mountains of the Kyrgyz Republic and Tajikistan are the water towers for many rivers in Central Asia, and they are the major source of water supply for lowland countries such as Uzbekistan [9,10]. The Kyrgyz Republic contains about 45% of all glaciers in Central Asia [11], and 4% of the country is under permanent ice and snow. Rivers are the major water resources in Central Asia, and most of them are transboundary [2]. Mountains in the region are the primary source of water for rivers and agricultural practices.

Central Asia is a seismically active region [12]. One consequence is that inhabitants of the region are vulnerable to mass movements, particularly mudflows. These may begin as surface erosion and sediment transport to valley basins. Sediments accumulate in toe slopes and can be mobilized by flash floods, damaging downstream infrastructure and threatening people. Forests in the region have mainly a protective role, contributing to combating desertification and preventing natural disasters (e.g., mudflows, floods, and droughts). Mountain forests are particularly important for water supply, but the disturbance of mountain forests in Central Asia through overgrazing, illegal logging, drought, and wildfires [13,14] have altered forest hydrological processes and accelerated soil erosion, mudflows, landslides, and downstream flooding [15].

Uzbekistan is one of the arid countries in Central Asia, with about 90% of its surface water used for agriculture [11]. Most of the country (79% by area) is flat, comprised of semi-desert steppes or desert zones, which include desert areas in the far west that have formed as a result of the drying of the Aral Sea [16,17]. The southeastern areas have a continental climate, containing the high mountains forming part of the Tien Shan and Gissar–Alai Ranges. Despite the importance of mountain areas in regional hydrology, the body of literature investigating watershed hydrology and water quality in this country remains scarce. Uzbekov et al. [18] predicted the impacts of future climate change on streamflow in the Ugam River watershed, Uzbekistan, from 2019 to 2048 using the Soil and Water Assessment Tool (SWAT) model. These authors found that with a 1.4 °C increase in air temperature and a 286 mm decrease in precipitation, the streamflow in the watershed is expected to decrease by 42% within thirty years. Olsson et al. [19] assessed stream water quality in the Zerafshan River basin using measured data from 1980 to 2009 along with multivariate statistical analysis. They stated that water quality declines in the middle and lower reaches of the Zerafshan River due to the return flows from intense agricultural irrigation, industrial effluent, and municipal wastewater. Scott et al. [20] estimated the influence of irrigation water on the hydrology and water budgets of two small lakes in Khorezm, Uzbekistan. They collected surface and groundwater samples from the two lakes in June and July 2008 and analyzed for δ^2H, $\delta^{18}O$, and major ion contents. The groundwater table and lake surface elevations were monitored, and the local aquifer characteristics were determined through aquifer tests. These authors reported that lake evaporation was about 70 mm/d during the study period. Without surface water input, the water volume of the lakes may decrease dramatically, with potential to the point of complete desiccation. Although the above-limited studies provided some useful insights into the hydrology and water quality in Uzbekistan, a thorough literature search reveals that little effort has

been devoted to investigating the impacts of forest disturbance and changing climate on mountain hydrological processes using the SWAT model.

The goal of this study was to quantify the mountain hydrological processes in the Aktash River watershed (ARW), Uzbekistan. Our specific objectives were to: (1) develop a SWAT model for the ARW; (2) calibrate and validate the model with remote sensing data; (3) apply the model to estimate the ARW hydrological processes, including streamflow, surface runoff, evapotranspiration (ET), groundwater discharge, snowmelt, and water yield over the past 17 years from 2003 to 2019; and (4) ascertain the effects of land use and afforestation on hydrological processes in the ARW. This quantification is essential to water resource managers, farmers, and stakeholders in the region for developing better water resource management strategies and documenting the critical role of mountain forests in water resource management.

2. Materials and Methods

2.1. Study Site

The ARW is located 60 km from the capital Tashkent on the southern slope of Karzhantau, Uzbekistan (Figure 1). The elevation is 1100–1600 m above sea level, with approximately 71% of the slopes angled at 25°. The watershed has a mild climate with a hot and dry summer (average maximum temperature of 27.2 °C in July) and a cold winter (average minimum temperature of −3 °C between December and February) [21,22]. Based on the data downloaded from the World Weather for Water Data Service (W3S), University of Guelph, Canada (https://www.uoguelph.ca/watershed/w3s/, accessed on 4 July 2023), the average annual precipitation was 1164 mm from 2001 to 2019. Streams in the ARW are largely fed by snowmelt and stormwater. The average streamflow from 1947 to 1965 was 0.41 m^3/s, with a maximum of 7.1 m^3/s in March–April and a minimum of 0.08 m^3/s in August–January [9,23]. Streamflow gradually increases from September to February of the next year, with a peak discharge occurring in April–May. Based on the Google Earth database, the ARW consists of 22.90% forest land, 0.04% agricultural land, 1.81% urban land, and 75.26% rangeland, with a total area of 19.55 km^2. The ARW was further divided into 17 catchments in this study (Figure 1).

Beginning in 1898 through 1903 and then from 1910 to 1914, almost 700 ha of the lower watershed was afforested to reduce soil erosion and mudflows [24]. Slopes were terraced manually with ditch terraces and seedlings of broadleaves planted along the slope at a distance ranging from 35 to 50 cm. The dominant species planted were walnut, oak, and juniper, with an admixture of ash, maple, and elm. In addition, seeds of almond, pistachio, walnut, and oak were sown between the terraces. The very dense planting and dry climate have proven unfavorable for the growth and development of walnut, oak, and ash except on north-facing slopes (Figure 2), but openings have been filled by native species, including hawthorns. The success of this early afforestation effort can be seen in the reduction in mudflows and the summer flows of the streams, as compared to the relatively bare slopes of nearby watersheds.

2.2. SWAT Model for ARW

SWAT is a watershed- and basin-scale model for simulating the quality and quantity of surface and ground waters in conjunction with the impacts of land use, land management, and climate change. SWAT is widely used to assess watershed hydrological processes, soil erosion, non-point source pollution, and regional watershed management (https://swat.tamu.edu/, accessed on 4 July 2023). In this study, the ARW hydrological model was developed using ArcSWAT (https://swat.tamu.edu/software/arcswat/, accessed on 4 July 2023). The ArcSWAT is an ArcGIS-ArcView extension and interface for SWAT. The major steps in developing the SWAT-ARW model included: (1) Watershed delineation. This step involved the setup of a digital elevation model (DEM), the creation of stream networks, and the selection of watershed inlets or outlets using the ArcSWAT watershed delineation interface; (2) HRU (Hydrologic Response Unit) analysis. This process defined

soil types, land uses, slopes, and HRUs; and (3) Weather data preparation. This step included precipitation, air temperature, relative humidity, solar radiation, and wind speed data acquisitions and reclassifications.

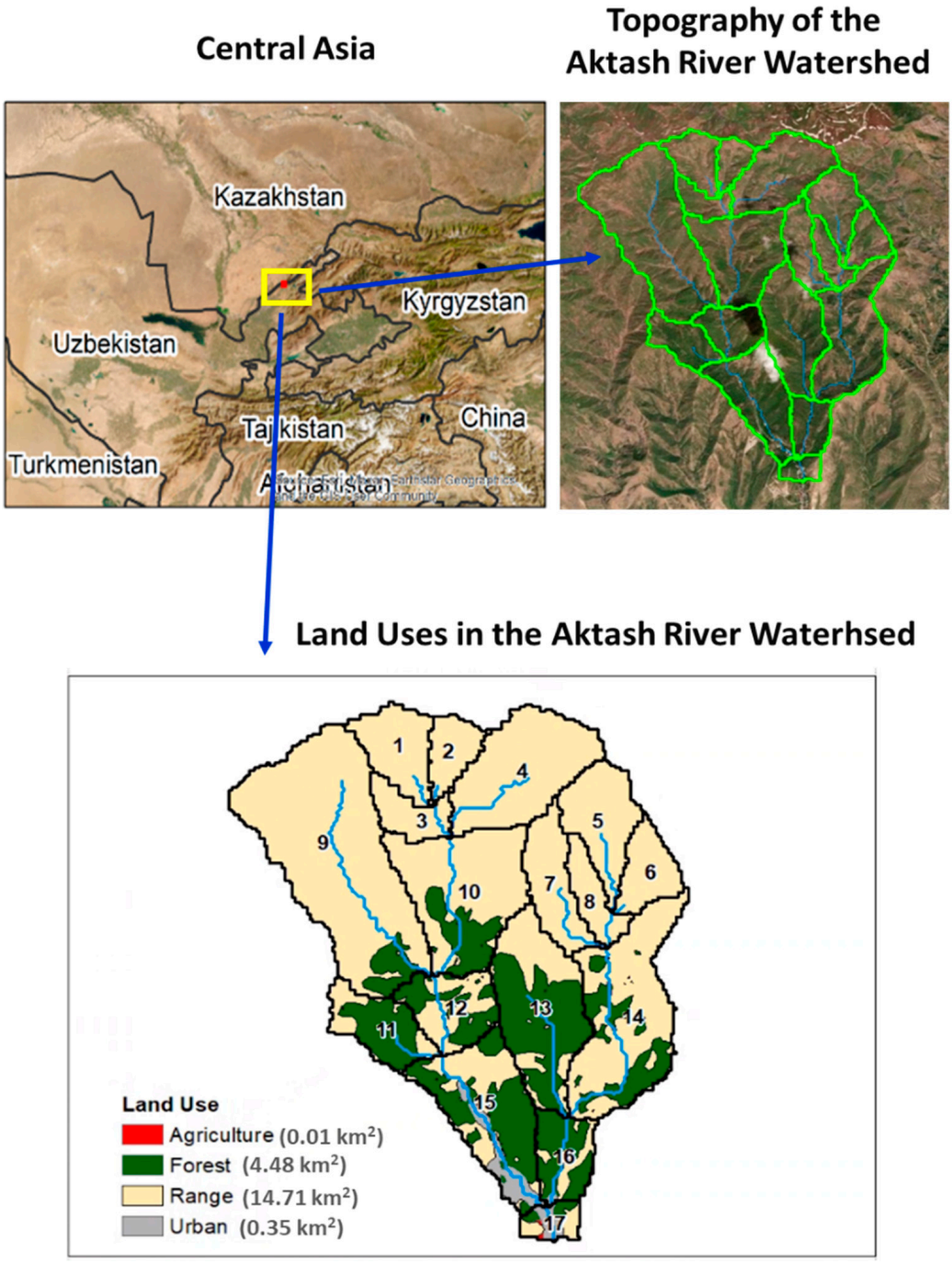


Figure 1. Location, land use, and topography of the Aktash River Watershed in Uzbekistan, Central Asia. The numbers in the figure denote the names of catchments.

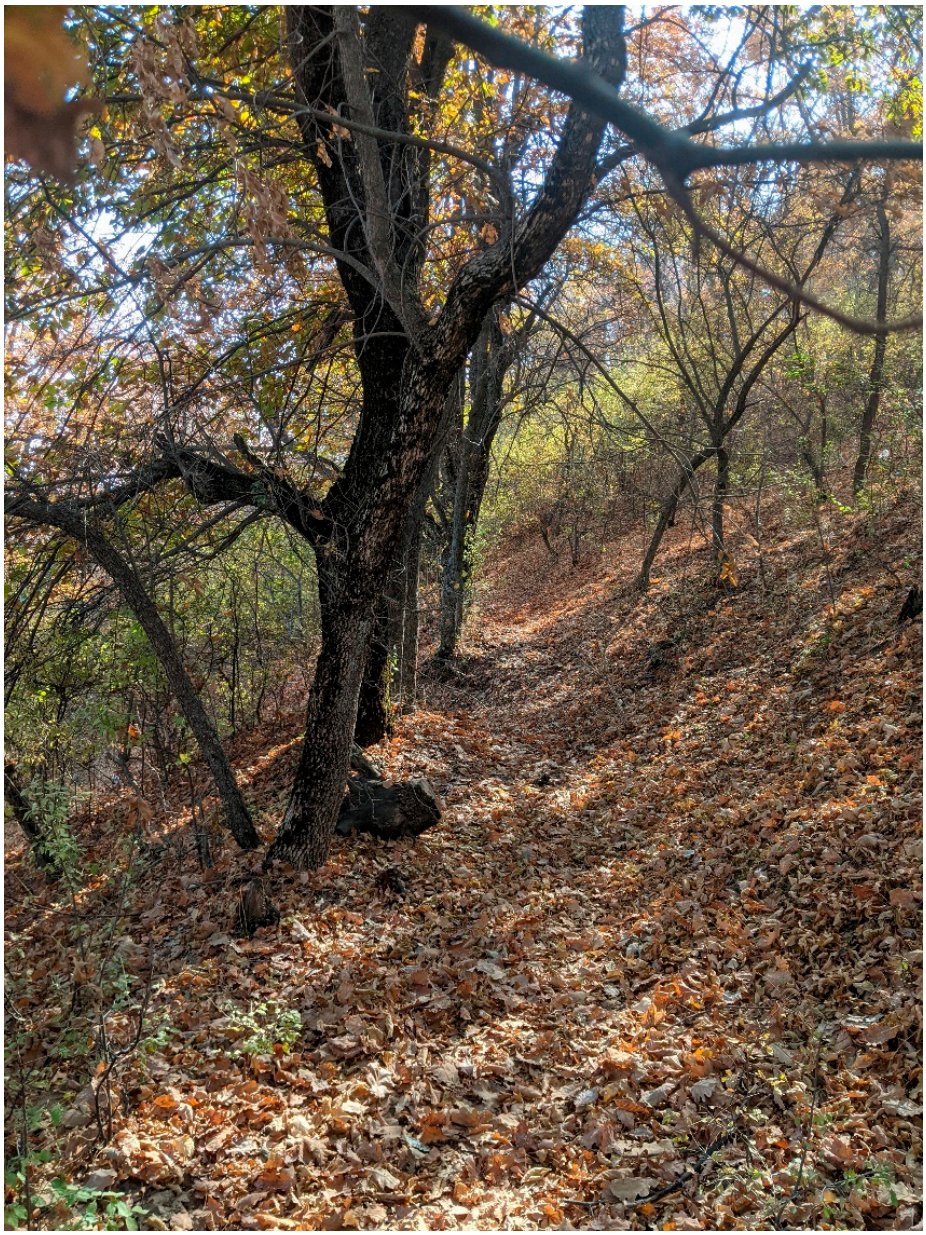


Figure 2. Planted oak, approximately 100 years old, in the mid-slope of the Aktash River Watershed. Note the trees were planted on the downside of the ridge created by terracing and the in-filling by naturally regenerating native species and direct seeding (Photo credit: John Stanturf).

2.3. Data Acquisition

The DEM data for the ARW–ArcSWAT model were obtained from Google Earth (https://earth.google.com/web/@41.57364703,64.23769421,463.91200418a,29707.8675831d,35y,0h,0t,0r, accessed on 4 July 2023) and converted to the format required by ArcSWAT. The soil and land-use/land-cover data were downloaded from the Europe/Asia Maps of the SWAT website (https://swat.tamu.edu/data/, accessed on 4 July 2023). Similarly, the daily weather data, including precipitation, maximum and minimum temperature, relative humidity, solar radiation, and wind speed, were downloaded from the World Weather for Water Data Service (W3S), University of Guelph, Canada (https://www.uoguelph.ca/watershed/w3s/, accessed on 4 July 2023). These datasets were further reformatted in compliance with the data formats required by ArcSWAT.

Little measured hydrological data are available for comparison with the SWAT–ARW model. In this study, we attempted to use the ET data obtained from remote sensing for this purpose. The 8-day ET data with a 500 m resolution were downloaded from MODIS (Moderate Resolution Imaging Spectroradiometer) or, more specifically, from MOD16A2 (https://modis.gsfc.nasa.gov/data/dataprod/mod16.php, accessed on 4 July 2023). MODIS is a satellite-based sensor used for earth and climate measurements.

2.4. Mann–Kendall Analysis

Annual trends of precipitation, surface runoff, ET, snowmelt, water yield, groundwater discharge, and streamflow over the past 17 years are determined using the Mann–Kendall analysis. Mann–Kendall statistics is a nonparametric trend test and is calculated as [25]:

$$S = \sum_{k=1}^{n-1} \sum_{j=k+1}^{n} \operatorname{sgn}(X_j - X_k) \tag{1}$$

with

$$\operatorname{sgn}(x) = \begin{cases} 1 & \text{if } x > 0 \\ 0 & \text{if } x = 0 \\ -1 & \text{if } x < 0 \end{cases} \tag{2}$$

The mean of S is zero, and the variance is

$$\sigma = \frac{1}{18}\{n(n-1)(2n+5) - \sum_{j=1}^{m} t_j(t_j-1)(2t_j+5)\} \tag{3}$$

where n is the number of times of measurements, *m* is the number of the tied groups in the data set, and t_j is the number of data points in the jth tied group. Kendall's S statistic is approximately normally distributed if the following Z-transformation is valid:

$$Z = \begin{cases} \frac{s-1}{\sigma} & if\ S > 0 \\ 0 & if\ S = 0 \\ \frac{s+1}{\sigma} & if\ S < 0 \end{cases} \tag{4}$$

The statistic S is closely related to Kendall's τ as:

$$\tau = \frac{S}{D} \tag{5}$$

with

$$D = \left[\frac{1}{2}n(n-1) - \frac{1}{2}\sum_{j=1}^{p} t_j(t_j-1)\right]^{1/2} \left[\frac{1}{2}n(n-1)\right]^{1/2} \tag{6}$$

In this study, the Mann–Kendall analysis is implemented with Kendall's package in R-Statistics [26].

3. Results

3.1. Model Calibration and Validation

A watershed model calibration is to match the model predictions with field measurements for a period (e.g., 10 years) by adjusting input parameter values within an acceptable range, whereas a watershed model validation compares the model predictions with field measurements for another period (e.g., another 10 years) without changing any input parameter values. In this study, we used the ET data from remote sensing as surrogates for field measurements for the model calibration and validation because no other measured hydrological data exist in the ARW. Table 1 lists the major input parameter values used during the model calibration.

Table 1. Major input parameter values used for the ARW model.

Parameter	Definition	Value	Unit/Method/ Explanation	Reference
SFTMP	Snowfall temperature	1	°C	Local observation
SMTMP	Snowmelt base temperature	0.5	°C	Local observation
SMFMX	Melt factor for snow on June 21	4.5	mm H_2O/°C-day	Local observation
SMFMN	Melt factor for snow on December 21	4.5	mm H_2O/°C-day	Local observation
TIMP	TIMP: Snowpack temperature lag factor	1		Local observation
IPET	Potential evapotranspiration (PET) method	1	Penman–Monteith method	Calibrated
ESCO	Soil evaporation compensation factor	0.9		Calibrated
EPCO	EPCO: Plant uptake compensation factor	1		Calibrated
ICN	Daily curve number calculation method	0	Calculate daily CN value as a function of soil moisture	Calibrated
CNCOEF	Plant ET curve number coefficient	1		Calibrated
ICRK	Crack flow code	0	Do not model crack flow in soil	Local observation
SURLAG	Surface runoff lag time	4	Days	Calibrated
CN2	Subbasins curve number	10%	CN2 increased by 10% for all subbasins	Calibrated
IRTE	Channel water routing method	0	Variable Storage Method	Calibrated
MSK_COL1	Calibration coefficient used to control the impact of the storage time constant for normal flow	0.75		Calibrated
MSK_COL2	Calibration coefficient used to control the impact of the storage time constant for low flow	0.25		Calibrated
MSK_X	Weighting factor controlling relative importance of inflow rate and outflow rate in determining water storage in reach segment	0.2		Calibrated
TRNSRCH	Fraction of transmission losses from the main channel that enter the deep aquifer	0		Calibrated
EVRCH	Reach evaporation adjustment factor	1		Calibrated
IDEG	Channel degradation code	0	Channel dimension is not updated as a result of degradation	Local observation
PRF	Peak rate adjustment factor for sediment routing in the main channel	0		Calibrated

Table 1. *Cont.*

Parameter	Definition	Value	Unit/Method/ Explanation	Reference
SPCON	Linear parameter for calculating the maximum amount of sediment that can be re-entrained during channel sediment routing	0.0001		Calibrated
SPEXP	Exponent parameter for calculating sediment re-entrained in channel sediment routing	1		Calibrated

Figure 3a compares the MODIS-measured with the SWAT-predicted daily ETs for an 11-year simulation period from 2002 to 2012. The values of R^2, Nash–Sutcliffe Efficiency (NSE), and percent bias (PBIAS) were, respectively, 0.66, 0.06, and 20.63. The NSE was low, but the R^2 and PBIAS were reasonably good. A plot of the MODIS-measured and SWAT-predicted peaks and valleys of the daily ETs shows that the predicted values were within the range of the measured ones graphically (Figure 3b). In this comparison, the 8-day ET with a 500 m resolution from MODIS was divided by eight to obtain an average daily ET. This average daily ET may not well represent the actual daily ET at the ARW as a dramatic variation in daily ET could occur within 8 days. In other words, there were uncertainties in the ET data from the MODIS measurement and SWAT modeling [27–29]. Nonetheless, the SWAT-predicted daily ETs compared reasonably well with the MODIS-measured daily ETs because they are within the range with good R^2 and PBIAS.

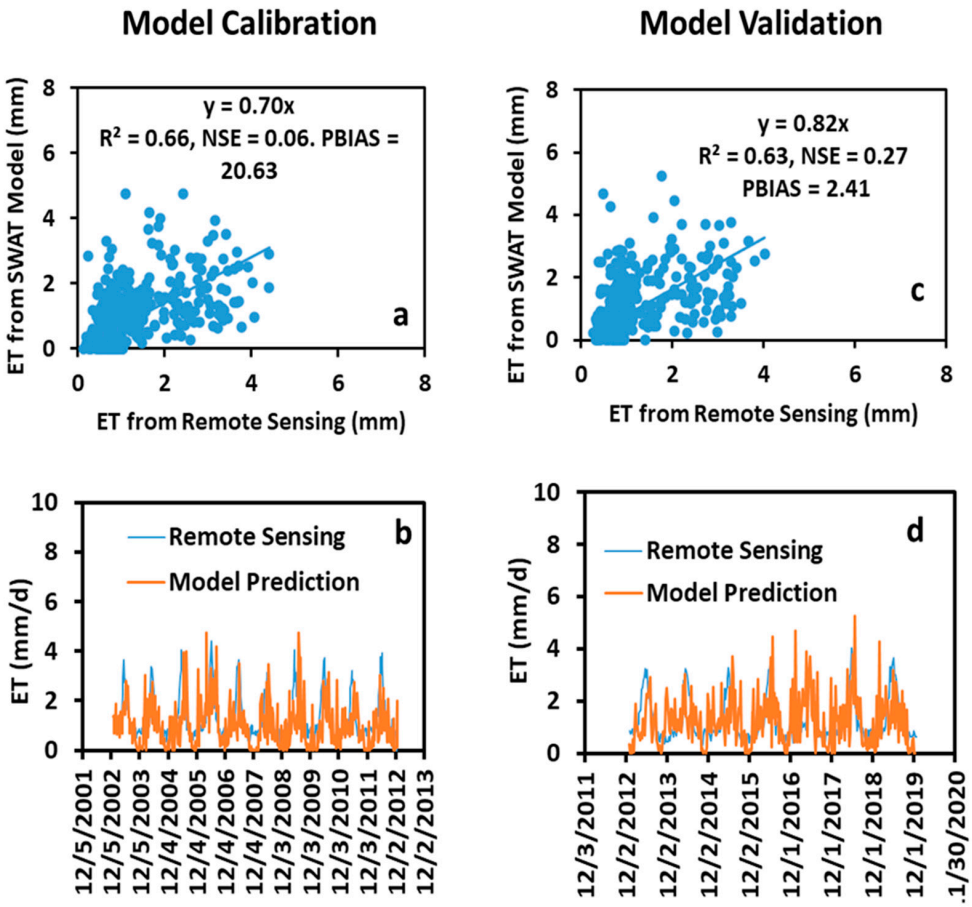


Figure 3. Comparisons of the MODIS-measured and SWAT-predicted daily ETs during the model calibration (**a**,**b**) and validation (**c**,**d**).

A comparison of the MODIS-measured with the SWAT-predicted daily ETs during the model validation from 2013 to 2019 is shown in Figure 3c. With the good R^2 (0.63), improved NSE (0.27), and better PBIAS (2.41), we concluded that a good agreement was obtained between the MODIS-measured and the SWAT-predicted daily ETs during the model validation. Visual estimation of the peaks and valleys of the daily ETs supported this conclusion (Figure 3d).

3.2. Daily, Monthly, and Annual Hydrological Processes

Daily variations in precipitation, surface runoff, and streamflow over the past 17-year simulation period from 2003 to 2019 at the ARW are shown in Figure 4. The daily precipitation was the model input data, whereas the daily surface runoff and streamflow were the simulation results. In general, the daily surface runoff (Figure 4b) corresponded reasonably well with the daily precipitation (Figure 4a). For instance, the daily surface runoff was 77.5 mm on 28 August 2006, when the daily precipitation was 121 mm, whereas the daily surface runoff was 6.2 mm on 3 April 2012, when the daily precipitation was 26.3 mm.

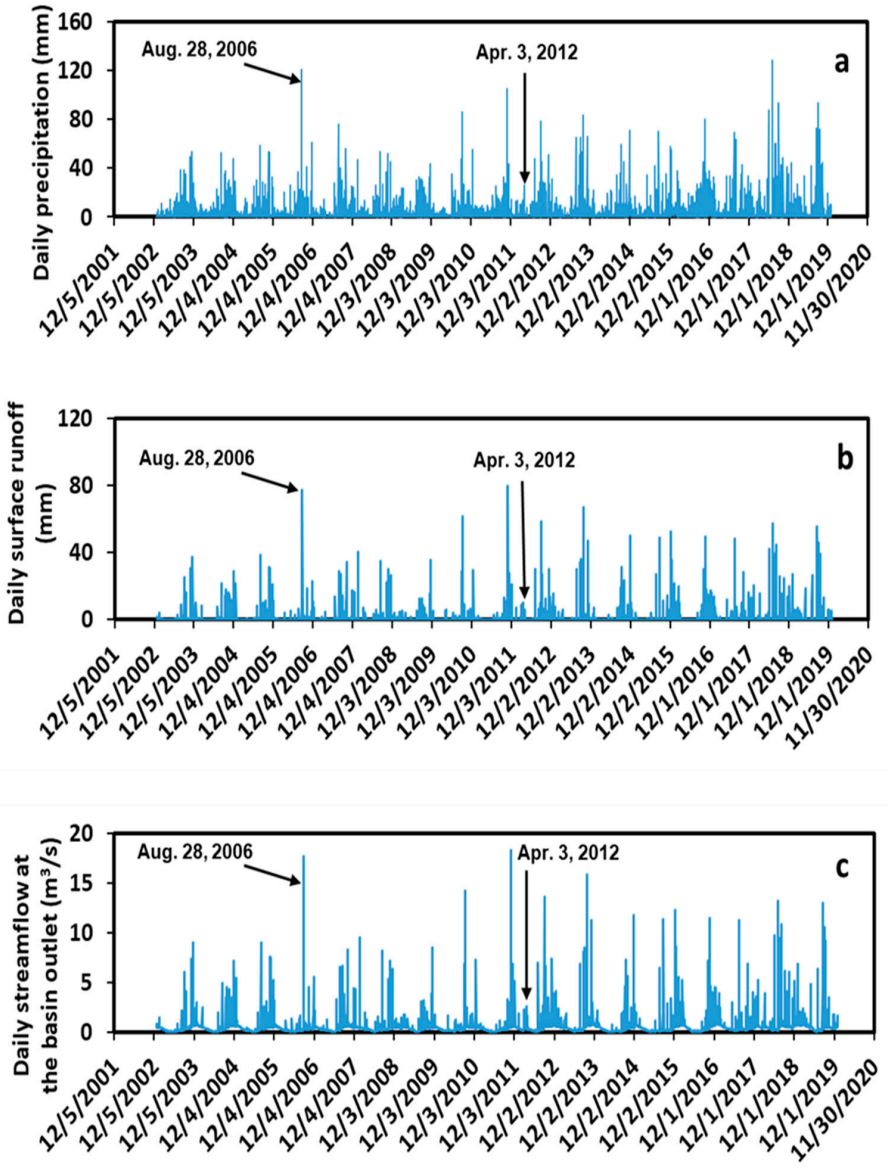


Figure 4. Daily precipitation (**a**), surface runoff (**b**), and streamflow (**c**) at the ARW. The daily precipitation was the model input data, while the daily surface runoff and streamflow were the model simulation results.

A plot of daily precipitation and surface runoff yielded the following linear equation:

$$Y_{runoff} = 0.46X_{prec} - 0.7 \ (R^2 = 0.75) \quad (7)$$

where Y_{runoff} is the surface runoff, and X_{prec} is the precipitation. This linear correlation indicated that about 46% of the daily precipitation contributed to the daily surface runoff at the ARW. This occurred because the daily surface runoff depended not only on precipitation but also on watershed conditions such as antecedent soil water content, watershed slope, and land cover.

A similar pattern was observed between the daily streamflow and the daily precipitation. That is, the daily streamflow was 17.7 m^3/s on 28 August 2006 (Figure 4c) when the daily precipitation was 121 mm, while the daily streamflow was 1.63 m^3/s on 3 April 2012 when the daily precipitation was 26.3 mm. A plot of daily precipitation and streamflow yielded:

$$Y_{sflow} = 0.11X_{prec} - 0.18 \ (R^2 = 0.73) \quad (8)$$

where Y_{sflow} is the streamflow. The result demonstrated the daily streamflow had a good linear correlation with the daily precipitation. This pattern was also reported by Ouyang [30] for a watershed in Mississippi, USA. The simulated average daily streamflow from 2003 to 2019 at the ARW was 0.52 m^3/s, which was consistent with the observed average daily streamflow of 0.41 m^3/s from 1947 to 1965 at the same basin [23]. Unlike daily surface runoff and streamflow, the patterns of the daily ET, groundwater discharge (to streams), snowmelt, and water yield did not correspond to the pattern of the daily precipitation (Figure 5) because these hydrological variables were affected by other surficial and geological factors in addition to the precipitation, such as temperature, snowfall, topography, and soil type. The daily ET showed a typical pattern, increasing from winter to spring, reaching its maximum in summer, and decreasing from fall to the next winter (Figure 5a). The average and maximum daily ET were 1.11 and 8.5 mm, respectively, in winter and spring. These values were compatible with those observed from remote sensing, which had the average and maximum daily ET of 1.24 and 4.41 mm in winter and spring, respectively.

The opposite pattern was found for the daily groundwater discharge, increasing from summer through fall, reaching the maximum in winter, and then decreasing from spring to the next summer (Figure 5b). This occurred because of snowmelt during winter (Figure 5c). Obviously, the snowmelt was a major factor in groundwater discharge into the streams of the ARW. The average and maximum daily groundwater discharges were 1.05 and 2.71 mm, respectively, while the average and maximum daily snowmelt were 0.38 and 35.9 mm, respectively. A comparison of Figure 5d with Figure 4a revealed that the daily water yield corresponded well with the daily precipitation. In other words, an increase in the daily precipitation increased the daily water yield. The average and maximum daily water yield were 2.29 and 82.1 mm, respectively. Monthly changes in average precipitation, surface runoff, ET, snowmelt, water yield, groundwater discharge, and streamflow from 2003 to 2019 at the ARW are shown in Figure 6. The wet months occurred from July to December, and the dry months from January to June. The monthly surface runoff followed the same pattern as the monthly precipitation (Figure 6a). This was because the surface runoff normally corresponded with the precipitation. In contrast, the monthly ET increased from January and attained the maximum in late summer (August) and then decreased to the minimum in December (Figure 6a) because the monthly ET depended not only on precipitation but also on air temperature throughout the year. Unlike the monthly ET, the monthly snowmelt, water yield, and groundwater discharge were zero or lowest during the summer months (Figure 6b). A similar pattern was also observed for the monthly streamflow.

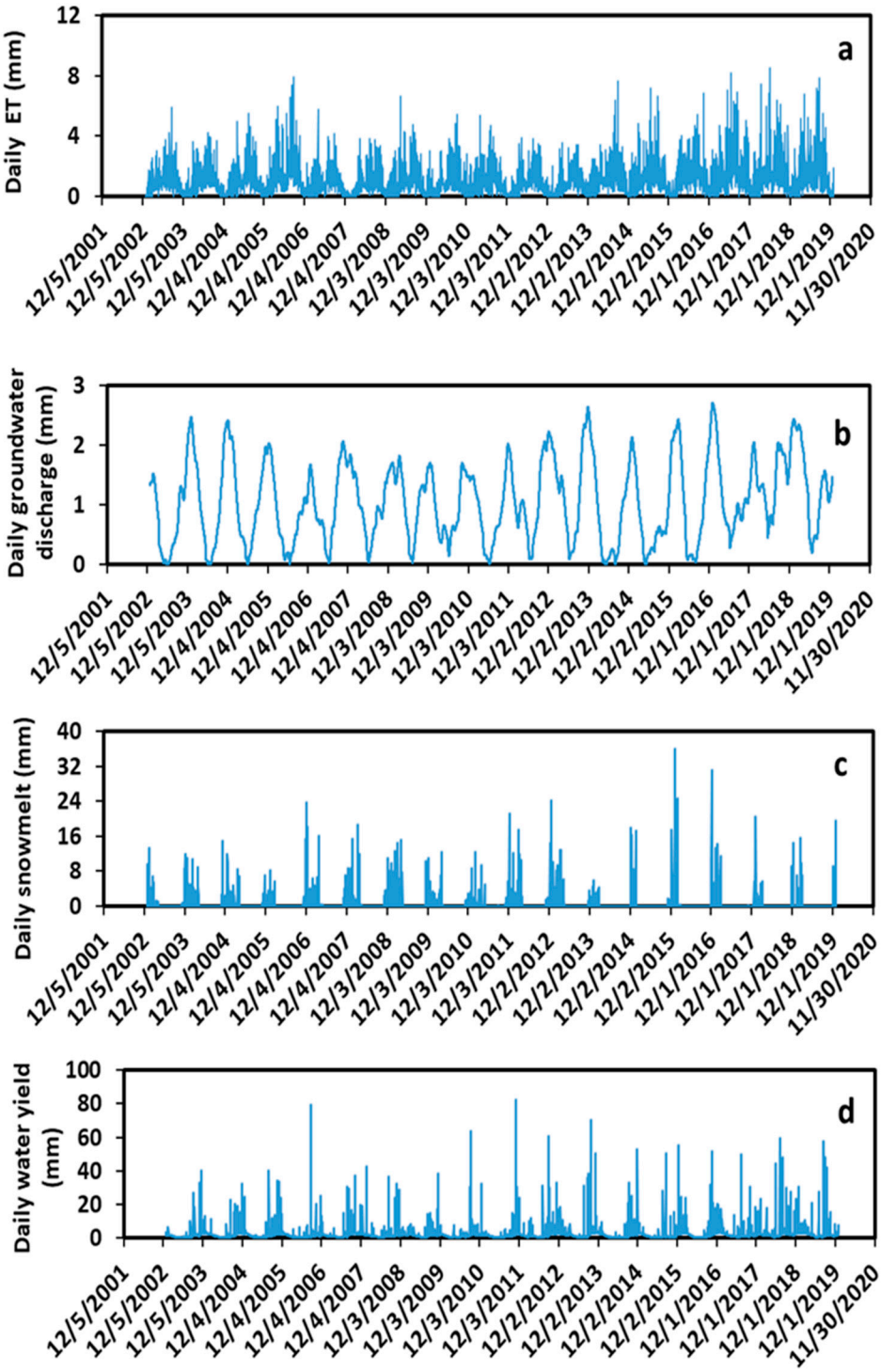


Figure 5. Simulated daily ET (**a**), groundwater discharge (**b**), snowmelt (**c**), and water yield (**d**).

Seasonal variations of the hydrological processes are given in Table 2. They were in the following order: fall > summer > winter > spring for precipitation and surface runoff; summer > spring > fall > winter for ET; winter > spring > fall > summer for snowmelt; fall > winter > summer > spring for water yield and streamflow; and winter > fall > spring > summer for groundwater discharge. This seasonality would provide useful information to farmers, foresters, and decision makers for better water resource management in the ARW and Central Asia.

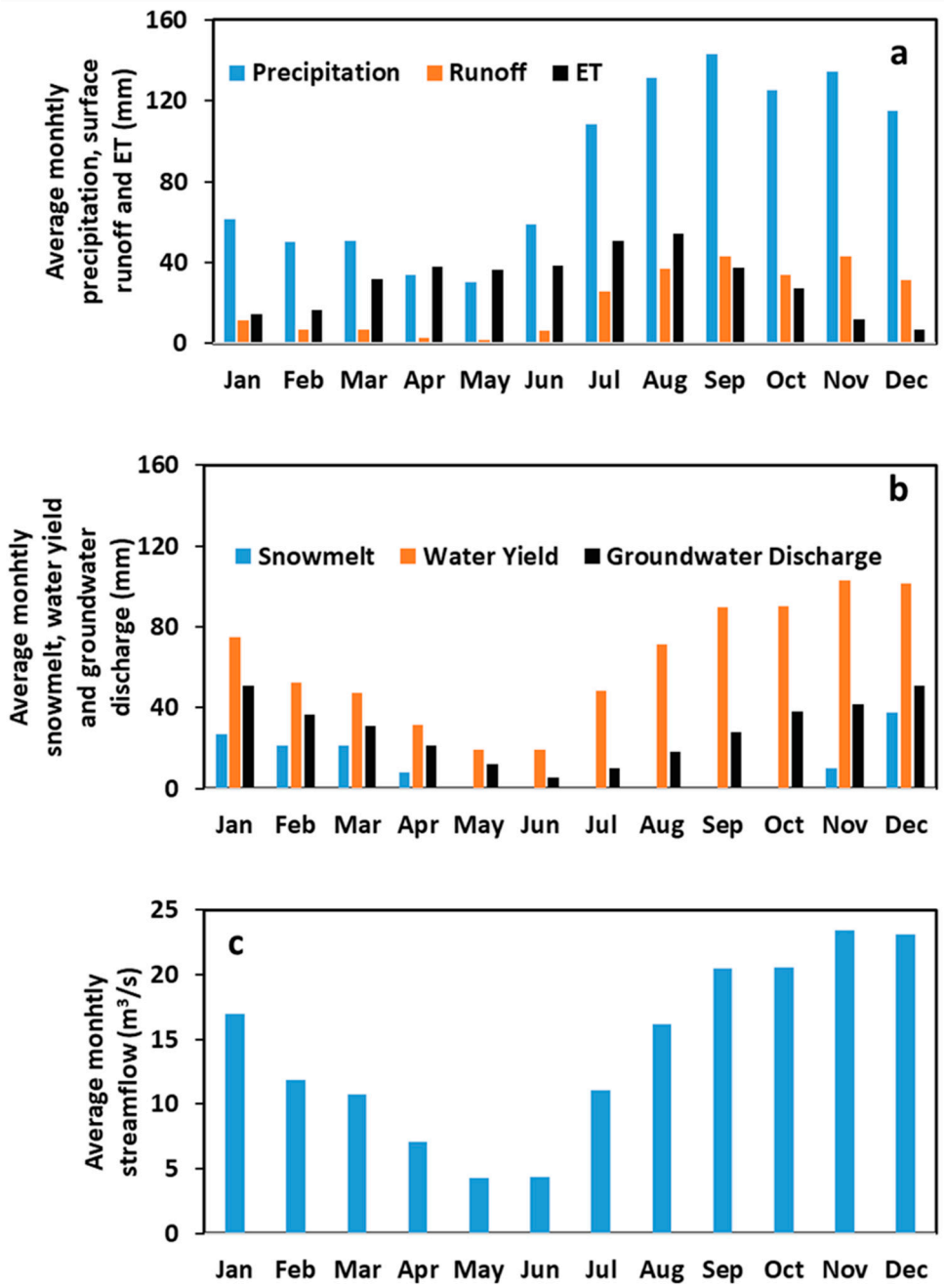


Figure 6. Monthly average precipitation, surface runoff, and ET (**a**); snowmelt, water yield, and groundwater discharge (**b**); and stream discharge (**c**).

Annual changes in precipitation, surface runoff, ET, snowmelt, water yield, groundwater discharge, and streamflow from 2003 to 2019 in the ARW are shown in Figure 7. While these hydrological processes varied from year to year, their annual averages followed the order: precipitation (1164 mm) > water yield (837 mm) > ET (407 mm) > groundwater discharge (384 mm) > surface runoff (278 mm) > streamflow (190 mm) > snowmelt (140 mm). The Mann–Kendall statistical test revealed a significantly increasing trend for the annual precipitation ($\tau = 0.45$, $p < 0.01$) and surface runoff ($\tau = 0.41$, $p < 0.02$) but not for the annual water yield ($\tau = 0.32$, $p = 0.08$), streamflow ($\tau = 0.32$, $p = 0.08$), or ET ($\tau = 0.32$, $p = 0.08$) over the past 17 years. The Mann–Kendall statistic τ ranges from -1 to 1 and measures the relationships between variables and times. If $\tau = 0$, no relationship exists, while $\tau = 1$ indicates an increasing trend, and -1 is a decreasing trend. The p-value is a statistical measure of a trend, and if $p \leq 0.05$, there is a monotonic trend [31].

Table 2. Seasonal averaged precipitation, surface runoff, snowmelt, water yield, groundwater discharge, and streamflow.

	Seasonal Average Precipitation (mm)	Seasonal Average Surface Runoff (mm)	Seasonal Average ET (mm)	Seasonal Average Snowmelt (mm)	Seasonal Average Water Yield (mm)	Seasonal Average Groundwater Discharge (mm)	Seasonal Average Streamflow (m^3/s)
Spring	115	11	106	29	98	64	22
Summer	298	69	143	0	139	34	32
Fall	403	120	76	10	283	107	65
Winter	226	49	38	85	229	138	52

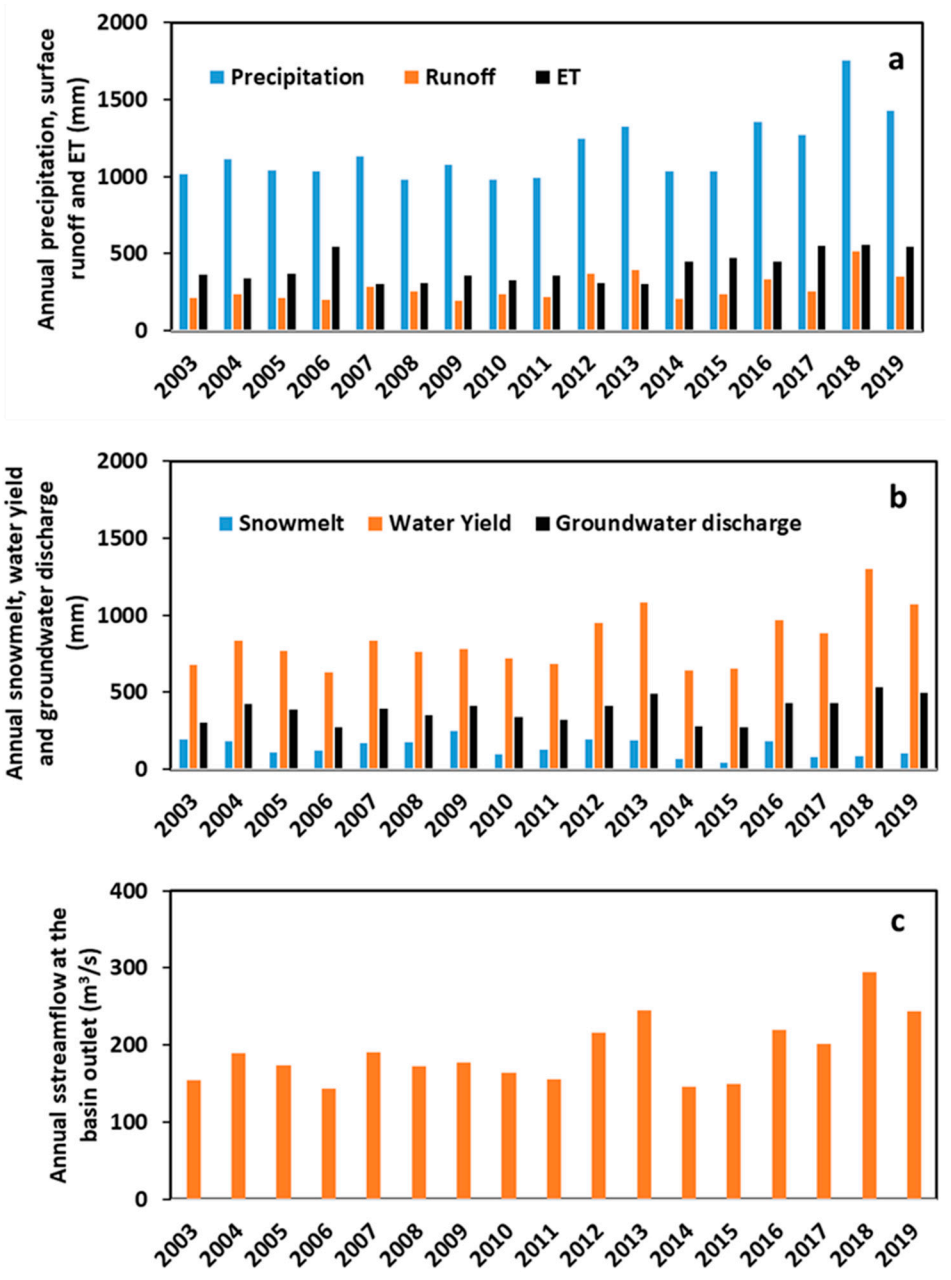


Figure 7. Annual precipitation, surface runoff, and ET (**a**); snowmelt, water yield, and groundwater discharge (**b**); and stream discharge (**c**).

3.3. Impacts of Land Use and Afforestation on Hydrological Processes

Impacts of land use and land cover (LULC) on ET, groundwater recharge (i.e., water flow from vadose zone soils and streams to aquifers), and water yield are shown in Figure 8. The major LULCs at the ARW included urban (URBAN, 0.35 km^2), agriculture (AGRL, 0.01 km^2), forest (FRST, 4.48 km^2), and range land (RNGE, 14.71 km^2). Figure 8a shows the annual average ET, groundwater recharge, and water yield from the urban, agriculture, forest, and rangeland. On average, they were in the following order: rangeland > forested land > urban > agricultural land for groundwater recharge and ET was rangeland > forested land > agricultural land > urban for water yield.

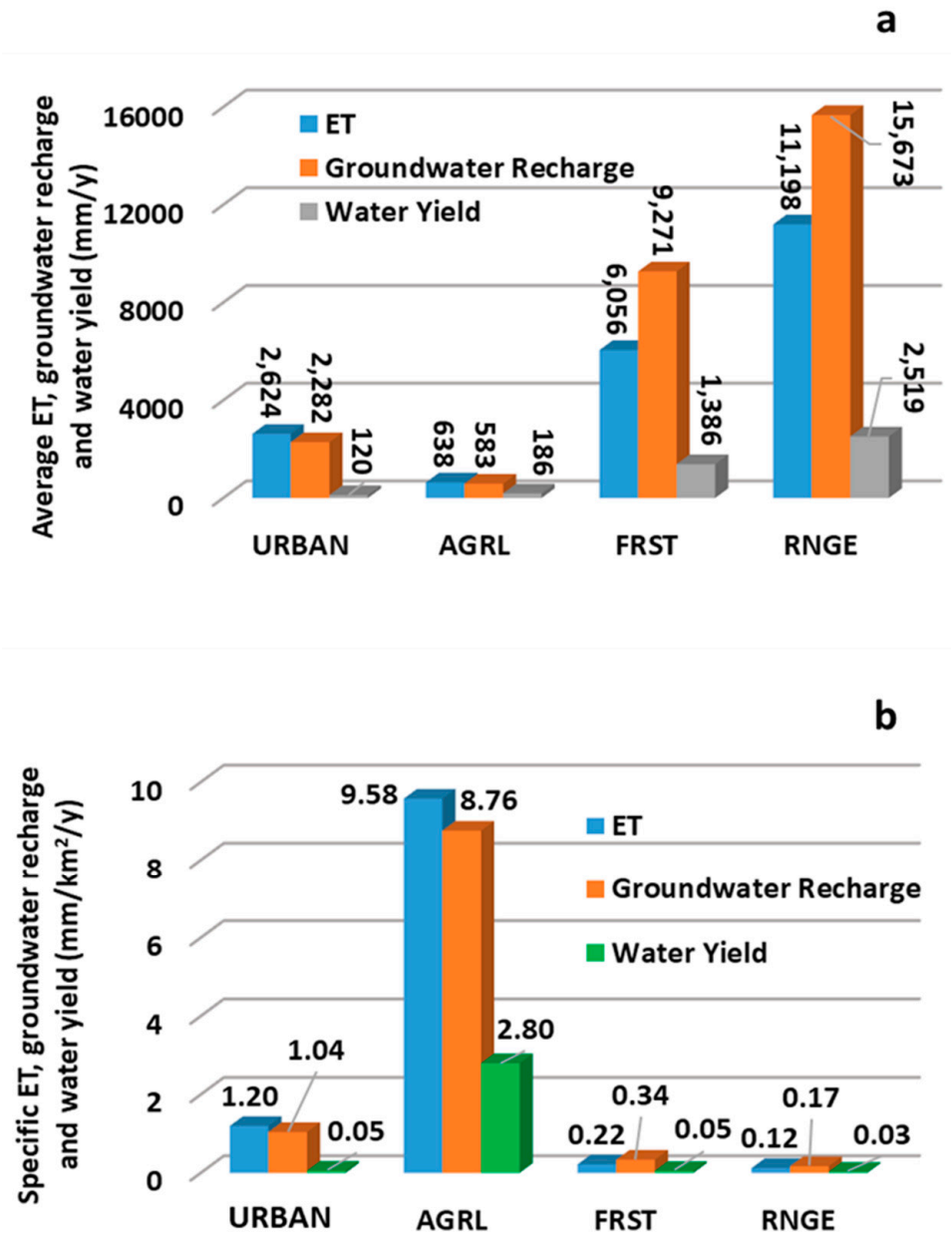


Figure 8. Impacts of urban (URBAN), agriculture (AGRL), forests (FRST), and range land (RNGE) on annual ET, groundwater recharge, and water yield.

Since the area varied with the land uses, it may not be easy to compare which land use had more effect on ET, groundwater recharge, and water yield. To circumvent this obstacle, we have used the unit area values of ET, groundwater recharge, and water yield for comparisons in this study. These unit area-specific values were obtained by dividing the

amount of the annual ET, groundwater recharge, and water yield by the corresponding area of each LULC. Results showed that agricultural land had much higher unit area-specific ET, groundwater recharge, and water yield than the other three land uses (Figure 8b).

A comparison of monthly and annual average precipitation, surface runoff, ET, water yield, and groundwater discharge between the afforested land-dominated catchment (Catchment 13) and the rangeland-dominated catchment (Catchment 14) is given in Table 3. Catchments 13 and 14 accounted, respectively, for 63.78% and 23.58% of the afforested land and 36.22% and 76.42% of the rangeland. There were no differences in precipitation and snowmelt between the two catchments. Approximately 20% more annual average surface runoff occurred in the rangeland-dominated catchment than in the afforested land-dominated catchment. A slight increase (0.13%) in water yield was observed in the rangeland-dominated catchment as compared to that of the afforested land-dominated catchment. In contrast, there were 0.08% and 4.86% more increases, respectively, in ET and groundwater recharge in the afforested land-dominated catchment than in the rangeland-dominated catchment.

Table 3. Monthly and annual average precipitation, surface runoff, ET, water yield, and groundwater discharge between Catchments 13 and 14. Catchment 13 has an area of 1.77 km^2 with 63.78% afforested land and 36.22% rangeland. Catchment 14 has an area of 2.16 km^2 with 23.58% afforested land and 76.42% rangeland.

Parameter	Monthly Average			Annual Average		
	Catchment 13 (Afforestation Dominated)	Catchment 14 (Rangeland Dominated)	Percent Different (%)	Catchment 13 (Afforestation Dominated)	Catchment 14 (Rangeland Dominated)	Percent Different (%)
Precipitation (mm)	32.18	32.18	0.00	386.15	386.15	0.00
Runoff (mm)	2.15	2.58	20.30	25.76	30.99	20.30
ET (mm)	16.99	16.97	−0.08	203.85	203.68	−0.08
Snowmelt (mm)	13.59	13.59	0.00	163.07	163.07	0.00
Water Yield (mm)	12.71	12.72	0.13	152.49	152.68	0.13
Groundwater Discharge (mm)	6.17	5.87	−4.86	73.99	70.39	−4.86

4. Discussion

Uzbekistan is a low forest cover country; depending on the source, forest cover is between 7.2% and 7.5% and includes the low stature saxaul (e.g., *Haloxylon* spp.) forests. Most of the forests (69%) are managed for the protection of soil and water or for biodiverse conservation (31%) with some restricted uses, mainly for non-timber forest products [32]. The mountains are mostly (93%) eroded [33] due to grazing and xeric conditions. Precipitation on such slopes enhances soil erosion and increasingly leads to destructive mudflows. Climate change is projected to further threaten water security in Uzbekistan as increased temperatures lead to the rapid melting of glaciers elsewhere in the region, causing severe water shortages in the important Amu Darya and Syr Darya Rivers by mid-century [34]. Thus, understanding the hydrology of mountain watersheds in Uzbekistan, indeed throughout Central Asia, is critically important, and the scarcity of data is challenging.

Very few efforts have been devoted to characterizing the past hydrological processes in the watersheds of Uzbekistan using field measurements and watershed-scale models. The SWAT model developed for the ARW was the first of its kind in the region. The model was calibrated and validated using remote sensing data from MOD16A2 because no other field-measured data was available. It has been reported that data from MODIS may under- or over-estimate ET, depending on study locations [35–37]. Ha et al. [36] compared ET between eddy covariance measurements and MODIS estimates in a disturbed ponderosa pine forest in the semiarid area near Flagstaff, Arizona, USA. These authors conclude that

MODIS ET underpredicted annual eddy ET primarily due to underestimation of the leaf area index. Conrad et al. [35] estimated spatial and temporal patterns of water depletion in the irrigated land of Khorezm in the lower floodplain of the Amu Darya River, Central Asia. They reported that MODIS ET somewhat underestimated the measured crop ET, although they had a moderate linear correlation with $R^2 = 0.6$. Their study results were similar to our findings, i.e., the MODIS ETs from our study were 70% (Figure 3a) and 82% (Figure 3c) of the SWAT ETs, respectively, during the model calibration and validation. Qiao et al. [38] compared ET from SWAT and MODIS in grasslands of the southern Great Plains, USA, and concluded that the SWAT model produced better ET than that of the MODIS estimates. Therefore, our SWAT simulations were reasonable.

In general, daily surface runoff and streamflow closely responded to daily precipitation but were not proportionally correlated with it. A 4.6-fold decrease in the daily precipitation decreased the daily surface runoff and streamflow by more than 11 times. This occurred because the daily surface runoff and streamflow depended not only on the precipitation but also on the watershed conditions, highlighting the importance of sustainable land use practices for long-term water security. The projected increased intensity of precipitation events will increase the risk of mudflows in degraded (i.e., over-grazed) watersheds [39,40] that could be mitigated by afforestation.

The daily ET did not correlate to the daily precipitation and showed a typical seasonal pattern of increasing from winter to spring, reaching a maximum in summer, and decreasing from fall to the next winter. In contrast, the daily groundwater discharge increased from summer through fall, reached a maximum in winter, and then decreased from spring to the next summer. An increase in the daily precipitation increased the daily water yield. Average temperatures in Uzbekistan are projected to increase significantly faster than the projected global average. Under the most pessimistic scenario (the highest emissions pathway, RCP8.5), average temperatures are projected to rise by 4.8 °C by the end of the century [34].

Annual variations of the mountainous hydrological processes followed the order: precipitation (1164 mm) > water yield (837 mm) > ET (407 mm) > groundwater discharge (384 mm) > surface runoff (278 mm) > streamflow (190 mm) > snowmelt (140 mm). The Mann–Kendall statistical test revealed a significant increasing trend for the annual precipitation ($\tau = 0.45$, $p < 0.01$) and surface runoff ($\tau = 0.41$, $p < 0.02$) but not for the annual water yield ($\tau = 0.32$, $p = 0.08$), streamflow ($\tau = 0.32$, $p = 0.08$), and ET ($\tau = 0.32$, $p = 0.08$) over the past 17 years. Based on the specific-value comparison (i.e., amount per unit square kilometer per year), agricultural land had much higher ET, groundwater recharge, and water yield than the grassland, forest, and range lands.

Afforestation is a field process of growing trees in non-forest land to create forests. Afforestation can conserve precipitation water, diffuse surface runoff, and absorbs pollutants, which mitigates river flooding, reduces soil erosion, and produces clean water [41]. A 20% decrease in the monthly and annual average surface runoff in the afforestation-dominated land (Catchment 13) supports the conclusion that growing trees prevent surface water runoff and, thereby, soil erosion. A 4.86% increase in monthly and annual average groundwater recharge in the afforestation-dominated land revealed that afforestation enhanced groundwater recharge as compared to that of the rangeland in the ARW.

5. Conclusions

A site-specific SWAT model was developed to quantify the mountain hydrological processes in the Aktash River watershed of Uzbekistan, Central Asia. The model was calibrated and validated using remote sensing ET data from the MODIS with reasonable agreements, although the MODIS ET somewhat underestimated the SWAT ET. Additionally, our SWAT estimated ETs were comparable to those reported by others at the Amu Darya River, Central Asia.

Daily streamflow and surface runoff corresponded reasonably well with daily precipitation, but they were not proportionally correlated with daily precipitation because of the complex watershed conditions.

The patterns of daily ET, groundwater discharge, snowmelt, and water yield did not correspond to the pattern of the daily precipitation because these hydrological processes were affected by other surficial and geological factors in addition to precipitation.

The magnitudes of the seasonal hydrological processes followed the order: fall > summer > winter > spring for precipitation and surface runoff; summer > spring > fall > winter for ET; winter > spring > fall > summer for snowmelt; fall > winter > summer > spring for water yield and streamflow; and winter > fall > spring > summer for groundwater discharge.

Agricultural land had much higher specific values ($mm/km^2/y$) of ET, groundwater recharge, and water yield than those of urban, forest, and range lands. As compared to rangeland, afforested land reduced surface runoff and increased groundwater recharge, although the afforested land increased ET and decreased water yield slightly.

Our research findings on the mountainous hydrological processes provide useful information to farmers, foresters, and decision makers for better water resource management in the ARW, Central Asia, and other mountain watersheds with similar conditions.

Further study is warranted to perform field measurements of hydrological processes such as streamflow and surface runoff at the ARW for rigorously validating the SWAT model and for a comprehensive understanding of the mountainous hydrological processes at the ARW and Central Asia.

Author Contributions: Conceptualization, Y.O. and J.A.S.; methodology, Y.O.; validation, Y.O., J.A.S. and E.B.; formal analysis, Y.O.; investigation, Y.O. and J.A.S.; resources, Y.O. and M.D.W.; data curation, Y.O., M.D.W., J.A.S. and E.B.; writing—original draft preparation, Y.O.; writing—review and editing, Y.O., J.A.S., M.D.W., E.B. and P.M. All authors have read and agreed to the published version of the manuscript.

Funding: This research received no external funding.

Institutional Review Board Statement: Not applicable.

Informed Consent Statement: Not applicable.

Data Availability Statement: Data will be available from the authors upon reasonable request.

Acknowledgments: Not applicable.

Conflicts of Interest: The author declares no conflict of interest.

References

1. Ouyang, Y. New insights on evapotranspiration and water yield in crop and forest lands under changing climate. *J. Hydrol.* **2021**, *603*, 127192. [CrossRef]
2. Bekturganov, Z.; Tussupova, K.; Berndtsson, R.; Sharapatova, N.; Aryngazin, K.; Zhanasova, M. Water Related Health Problems in Central Asia—A Review. *Water* **2016**, *8*, 219. [CrossRef]
3. Cowan, P.J. Geographic usage of the terms middle Asia and Central Asia. *J. Arid. Environ.* **2007**, *69*, 359–363. [CrossRef]
4. O'Hara, S.L. Central Asia's water resources: Contemporary and future management issues. *Int. J. Water Resour. Dev.* **2000**, *16*, 423–441. [CrossRef]
5. USAID. Climate Risk Profile: Central Asia. 2023. Available online: https://www.preventionweb.net/publication/climate-risk-profile-central-asia (accessed on 18 February 2023).
6. Frenken, K. *Food and Agriculture Organization of the United Nations. Irrigation in Central Asia in Figures: AQUASTAT Survey-2012*; Food and Agriculture Organization of the United Nations: Rome, Italy, 2013.
7. Yin, Z.Y.; Wang, H.L.; Liu, X.D. A Comparative Study on Precipitation Climatology and Interannual Variability in the Lower Mid latitude East Asia and Central Asia. *J. Clim.* **2014**, *27*, 7830–7848. [CrossRef]
8. Broka, S.; Giertz, Å.; Christensen, G.; Rasmussen, D.; Morgounov, A.; Fileccia, T.; Rubaiza, R. Kazakhstan Agricultural Sector Risk Assessment. 2016. Available online: https://documents1.worldbank.org/curated/en/422491467991944802/pdf/103076-WP-KZ-P154004-Box394863B-PUBLIC-ASRA.pdf (accessed on 4 July 2023).
9. Abdukhalilovich, K.A. Agroforest Reclamation Fundamentals of Soil Erosion Control in the Mountains of the Uzbek SSR. Ph.D. Thesis, Agrarian University, Tashkent, Uzbekistan, 1984; 504p.

10. Shahgedanova, M.; Afzal, M.; Hagg, W.; Kapitsa, V.; Kasatkin, N.; Mayr, E.; Rybak, O.; Saidaliyeva, Z.; Severskiy, I.; Usmanova, Z. Emptying Water Towers? Impacts of Future Climate and Glacier Change on River Discharge in the Northern Tien Shan, Central Asia. *Water* **2020**, *12*, 627. [CrossRef]
11. Sorg, A.; Bolch, T.; Stoffel, M.; Solomina, O.; Beniston, M. Climate change impacts on glaciers and runoff in Tien Shan (Central Asia). *Nat. Clim. Chang.* **2012**, *2*, 725–731. [CrossRef]
12. Mavlyanova, N.G.; Lipatov, V.A.; Tiefenbacher, J.P. Regional Cooperative Disaster Risk Management in Central Asian Borderlands. *J. Borderl. Stud.* **2023**, *38*, 417–439. [CrossRef]
13. Khan, F.; Sohail, Z.; Khan, T.; Fatima, B.; Malik, F.; Bukhari, S.F.H.; Imadi, S.R.; Gul, A. *Vegetation of Central Asia and Environs*; Springer International Publishing: Cham, Switzerland, 2018; pp. 73–117.
14. Kleine, M.; Colak, A.; Kirca, S.; Sagheb-Talebi, K.; Orozumbekov, A.; Lee, D. Rehabilitating degraded forest landscapes in West and Central Asia. *IUFRO World Ser.* **2009**, *20*, 5–26.
15. United Nations Development Programme (UNDP). *Central Asia Human Development Report*; UN Development Programme: Bratislava, Slovakia, 2005; p. 246. Available online: https://digitallibrary.un.org/record/578152 (accessed on 4 July 2023).
16. Micklin, P. The past, present, and future Aral Sea. *Lakes Reserv. Res. Manag.* **2010**, *15*, 193–213. [CrossRef]
17. Micklin, P.; Aladin, N.V.; Chida, T.; Boroffka, N.; Plotnikov, I.S.; Krivonogov, S.; White, K. *Large Asian Lakes in a Changing World: Natural State and Human Impact*; Mischke, S., Ed.; Springer International Publishing: Cham, Switzerland, 2020; pp. 109–141.
18. Uzbekov, U.; Pulatov, B.; Alikhanov, B.; Pulatov, A. Predicting the impact of future climate change on streamflow in the Ugam River watershed. *Geoscape* **2021**, *15*, 159–172. [CrossRef]
19. Olsson, O.; Gassmann, M.; Manig, N.; Ikramova, M.; Wegerich, K. Basin efficiency approach and its effect on streamflow quality, Zerafshan River Uzbekistan. *J. Hydrol.* **2013**, *476*, 128–135. [CrossRef]
20. Scott, J.; Rosen, M.R.; Saito, L.; Decker, D.L. The influence of irrigation water on the hydrology and lake water budgets of two small arid-climate lakes in Khorezm, Uzbekistan. *J. Hydrol.* **2011**, *410*, 114–125. [CrossRef]
21. Ghimire, U.; Akhtar, T.; Shrestha, N.K.; Paul, P.K.; Schurz, C.; Srinivasan, R.; Daggupati, P. A Long-term Global Comparison of IMERG and CFSR with Surface Precipitation Stations. *Water Resour. Manag.* **2022**, *36*, 5695–5709. [CrossRef]
22. Huffman, G.J.; Bolvin, D.T.; Braithwaite, D.; Hsu, K.; Joyce, R.; Xie, P.; Yoo, S.-H. NASA Global Precipitation Measurement (GPM) Integrated Multi-Satellite Retrievals for GPM (IMERG). Algorithm Theoretical Basis Document (ATBD) Version 4. 2015. Available online: https://gpm.nasa.gov/sites/default/files/2020-05/IMERG_ATBD_V06.3.pdf (accessed on 4 July 2023).
23. Botman, K.S. Experience in Mountain Afforestation in Order to Combat Soil Erosion and Mudflows in the Aktash River Basin. Bachelor's Thesis, Agrarian University, Tashkent, Uzbekistan, 1968; p. 236.
24. Botman, E.K. *Survey of Anti-Erosion Plantings in the Aktashsay River Basin, Burchmullo Forestry Enterprise*; International Union of Forestry Research Organizations (IUFRO): Vienna, Austria, 2022.
25. Gilbert, R.O. *Statistical Methods for Environmental Pollution Monitoring*; John Wiley and Sons: New York, NY, USA, 1987.
26. Pohlert, T. Package "Trend". 2018. Available online: https://www.r-project.org/ (accessed on 4 July 2023).
27. Long, D.; Longuevergne, L.; Scanlon, B.R. Uncertainty in evapotranspiration from land surface modeling, remote sensing, and GRACE satellites. *Water Resour. Res.* **2014**, *50*, 1131–1151. [CrossRef]
28. Parajuli, P.B.; Risal, A.; Ouyang, Y.; Thompson, A. Comparison of SWAT and MODIS Evapotranspiration Data for Multiple Timescales. *Hydrology* **2022**, *9*, 103. [CrossRef]
29. Wambura, F.J. Uncertainty of drought information in a data-scarce tropical river basin. *J. Hydrol. Reg. Stud.* **2020**, *32*, 100760. [CrossRef]
30. Ouyang, Y. A Hybrid of Copula Prediction and Time Series Computation to Estimate Stream Discharge Based on Precipitation Data. *J. Am. Water Resour. Assoc.* **2022**, *58*, 471–484. [CrossRef]
31. Mangiafico, S.S. *Summary and Analysis of Extension Program Evaluation in R*, version 1.11.1; Rutgers Cooperative Extension: New Brunswick, NJ, Canada, 2016.
32. FAO. *Global Forest Resource Assessment*; Food and Agriculture Organization: Rome, Italy, 2020.
33. Kocherga, F. Research work on the fight with erosion of soils and flooding in the mountainous regions of Central Asia. In *Proceedings of the Central Asian Research Institute of Forestry Volume X*; Uzbekistan Publishers: Tashkent, Uzbekistan, 1966; pp. 16–57.
34. WB/ADB. *Climate Risk Country Profile: Uzbekistan, the World Bank Group and the Asian Development Bank*; World Bank Group: Washington, DC, USA, 2021.
35. Conrad, C.; Dech, S.W.; Hafeez, M.; Lamers, J.; Martius, C.; Strunz, G. Mapping and assessing water use in a Central Asian irrigation system by utilizing MODIS remote sensing products. *Irrig. Drain. Syst.* **2007**, *21*, 197–218. [CrossRef]
36. Ha, W.; Kolb, T.E.; Springer, A.E.; Dore, S.; O'Donnell, F.C.; Morales, R.M.; Lopez, S.M.; Koch, G.W. Evapotranspiration comparisons between eddy covariance measurements and meteorological and remote-sensing-based models in disturbed ponderosa pine forests. *Ecohydrology* **2015**, *8*, 1335–1350. [CrossRef]
37. Heinsch, F.A.; Zhao, M.S.; Running, S.W.; Kimball, J.S.; Nemani, R.R.; Davis, K.J.; Bolstad, P.V.; Cook, B.D.; Desai, A.R.; Ricciuto, D.M.; et al. Evaluation of remote sensing based terrestrial productivity from MODIS using regional tower eddy flux network observations. *IEEE Trans. Geosci. Remote Sens.* **2006**, *44*, 1908–1925. [CrossRef]
38. Qiao, L.; Will, R.; Wagner, K.; Zhang, T.; Zou, C. Improvement of evapotranspiration estimates for grasslands in the southern Great Plains: Comparing a biophysical model (SWAT) and remote sensing (MODIS). *J. Hydrol. Reg. Stud.* **2022**, *44*, 101275. [CrossRef]

39. Martel, J.-L.; Brissette, F.P.; Lucas-Picher, P.; Troin, M.; Arsenault, R. Climate change and rainfall intensity–duration–frequency curves: Overview of science and guidelines for adaptation. *J. Hydrol. Eng.* **2021**, *26*, 03121001. [CrossRef]
40. Siteur, K.; Eppinga, M.B.; Karssenberg, D.; Baudena, M.; Bierkens, M.F.; Rietkerk, M. How will increases in rainfall intensity affect semiarid ecosystems? *Water Resour. Res.* **2014**, *50*, 5980–6001. [CrossRef]
41. Ouyang, Y.; Leininger, T.D.; Moran, M. Impacts of reforestation upon sediment load and water outflow in the Lower Yazoo River Watershed, Mississippi. *Ecol. Eng.* **2013**, *61*, 394–406. [CrossRef]

Disclaimer/Publisher's Note: The statements, opinions and data contained in all publications are solely those of the individual author(s) and contributor(s) and not of MDPI and/or the editor(s). MDPI and/or the editor(s) disclaim responsibility for any injury to people or property resulting from any ideas, methods, instructions or products referred to in the content.